

DEVELOPMENT OF AN AUTOMATED SYSTEM FOR SUCCESSIVE IONIC LAYER ADSORPTION AND REACTION (SILAR) TECHNIQUE AT ROOM TEMPERATURE

DESARROLLO DE UN SISTEMA AUTOMATIZADO PARA LA TÉCNICA REACCIÓN Y ADSORCIÓN SUCESIVAS DE CAPAS IÓNICAS (SILAR) A TEMPERATURA AMBIENTE

E. MÁs-MOLINA^{a,b†}, J. ALBA-CABAÑAS^a, M. MUÑOZ-ARIAS^c, O. CRUZATA^d, M. SERRAPEDE^e, A. M. DÍAZ-GARCÍA^c, AND L. VAILLANT-ROCA^b

a) Physics Faculty, University of Havana, Cuba; ernesto.mas@fisica.uh.cu.†

b) Photovoltaic Research Laboratory, Institute of Materials Science and Technology-Physics Faculty, University of Havana, Cuba.

c) Inorganic and General Chemistry Department, Bioinorganic Laboratory, University of Havana, Cuba.

d) Laser Technology Laboratory, Institute of Materials Science and Technology, University of Havana, Cuba.

e) Politecnico di Torino, corso Duca degli Abruzzi 24, Torino, Italy. DISAT department.

† corresponding author

Recibido 17/11/2021; Aceptado 20/12/2022

In this work, we present the design, fabrication, and automation of a customized and affordable system capable of performing the thin film deposition techniques of Dip-Coating and SILAR at room temperature. To automate the system, parts from disused equipment were reused, new pieces were fabricated through additive manufacturing, and open-source software was also utilized. The device was controlled using an Arduino UNO R3. Additionally, a graphical interface was developed in Python with the PyQt library to adjust the motion settings and transmit parameters to the Arduino via serial communication. We validated the system by fabricating layers of Cu_2O and CuO , subsequently comparing their structural and morphological properties with findings previously reported in the literature.

En este trabajo presentamos el diseño, fabricación y automatización de un sistema personalizado y asequible, capaz de realizar las técnicas de deposición de capas delgadas *Dip-Coating* y *SILAR* a temperatura ambiente. Para la automatización, se reutilizaron partes de equipos en desuso, se fabricaron nuevas piezas mediante manufactura aditiva y, además, se empleó software de código abierto. El dispositivo se controló mediante un Arduino UNO R3. Además, se desarrolló una interfaz gráfica en Python con la biblioteca PyQt para ajustar la configuración del movimiento y transmitir parámetros al Arduino vía comunicación serial. Validamos el sistema mediante la fabricación de capas de Cu_2O y CuO , comparando posteriormente sus propiedades estructurales y morfológicas con los resultados reportados en la literatura.

PACS: Fabrication of nanostructures (fabricación de nanoestructuras), 81.07.-b; semiconductors film growth (crecimiento de capas semiconductoras), 68.55.ag; fabrication of semiconductors (fabricación de semiconductores), II-VI, 81.05.Dz; chemical synthesis (síntesis química), 81.20.Ka; heat treatments, effects on microstructure (tratamientos térmicos, efectos en la microestructura), 81.40.Gh.

I. INTRODUCTION

Deposition techniques for semiconductor thin films and nanostructures play a crucial role in scientific and technological applications. They enable the deposition of low-dimension materials onto substrates, facilitating the production of smaller and more compact electronics. Additionally, these techniques allow the growth of nanomaterials with diverse electrical, optical, and mechanical properties, which differ from those of bulk materials, enabling the development of high-performance devices [1].

The versatility of semiconductor thin film techniques lies in the ability to tune the properties of these films by controlling the composition and deposition parameters. This flexibility opens up opportunities for the development of novel devices. Just to name a few, the applications of thin films vary from optics, electronic and optoelectronic devices (reflective, anti-reflective, and anti-corrosive coatings, thin film transistors, integrated circuits, solar cells, photodetectors, LEDs, etc.) to magnetics and energy storage technologies (computer memories, supercapacitors, etc.) [2]. Exploring

these countless applications has led to the development of various techniques aimed at obtaining thin films tailored to specific purposes.

Deposition techniques can be subdivided into two categories: physical deposition and chemical deposition [3]. Physical deposition involves the transfer of a material, vaporized by physical processes (such as sputtering deposition, thermal evaporation, or electron beam evaporation), onto the substrate's surface [4]. In this type of deposition, the formation of the thin film typically occurs under controlled atmospheric conditions, often in a vacuum, and requires high temperatures or energy values. On the other hand, chemical deposition of thin films involves directing chemical precursors towards the substrate surface, initiating a reaction that forms a product layer or depositing materials dispersed in solvents, such as molecular precursors, and forming the layer after the solvent evaporates [5]. Chemical deposition heavily relies on factors like the chemistry of the solutions, pH value, viscosity, and other parameters [6].

While physical methods for producing thin films provide

excellent quality and high control over layer properties, they frequently involve notable constraints, such as requiring strict atmospheric control [7] and the use of sophisticated and costly equipment. On the other hand, chemical deposition techniques are widely used to produce thin films at low cost. These techniques are generally more cost-effective, simpler, and convenient for depositing a wide range of materials. For example, chemical deposition allows the formation of materials such as metal chalcogenides and metal oxides [6]. This versatility makes chemical deposition an attractive option for researchers and industries seeking to produce thin films and nanostructured materials with specific properties while keeping low costs and equipment requirements. Therefore, in this work, we focus on the development of chemical deposition methods systems like dip coating and successive ionic layer adsorption and reaction (SILAR) [8].

The dip coating method involves immersing the substrate vertically into a covering solution containing the dissolved material in a solvent. After a specified immersion time, the substrate is extracted from the solution at a constant speed to remove excess fluid. This process results in a thin liquid film, accomplished by various forces in equilibrium, such as viscous drag, gravitational forces, and surface tension within the concave meniscus shape [9]. The wet solvent is then evaporated to yield a dry thin film.

The SILAR process can be seen as a more complex version of the dip coating. This method involves sequential steps where the substrate is dipped into different beakers with precursor solutions. The film formation occurs through ions adsorption in one beaker and subsequent reactions with other ions in a different solution in a second beaker. Rinse recipients are used between steps to eliminate loosely attached ions. Each container can be at a different temperature, ensuring the proper pH value for the reaction. Figure 1 provides a visual guide to this process.

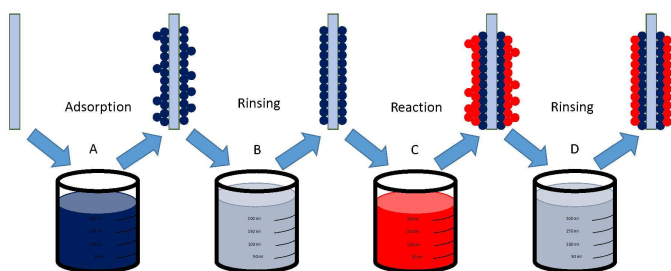


Figure 1. Diagram of one SILAR cycle. In step A the anions of the precursor solution are adsorbed by the substrate. During steps B and D the sample is rising in a solvent to eliminate not strongly attached ions. The last step involves immersing the substrate into reaction solution C to form the thin film.

The correct homogeneity in the coating of the layers obtained through these techniques is highly dependent on the precise control of immersion times and extraction speed in the precursor solutions [10]. It often takes a significant number of cycles to achieve the desired thickness of the material layer, which makes it difficult to perform manually.

To address this challenge, our objective was to develop, manufacture, and validate a cost-effective and customized

device capable of automating both the SILAR and dip coating techniques. These techniques share similar technological processes. Our goal in designing this unit was to streamline and optimize the production of coatings by providing precise control of immersion and extraction times, enabling the efficient production of high-quality coatings.

II. SYSTEM DETAILS

To explain the operational system of the device (Fig. 2), we will divide it into three subsystems: a mechanical lifter whose goal is to introduce the substrates into the precursor solution (Fig. 2a), a rotatory selector to choose the precursor solution to be used (Fig. 2b), and a control that enables communication between the computer and the device (Fig. 2c).

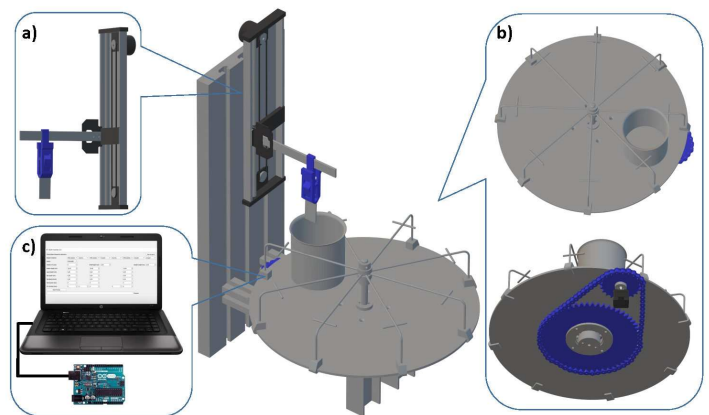


Figure 2. Representation of the system and each subsystem: a) Mechanism responsible for immersing the substrates in the precursor solution. b) Acrylic platform that holds the beakers containing the precursor solution to be used. c) Control unit that enables communication between the computer and the device.

II.1. Subsystem to introduce the substrates into the precursor solution (Figure 2a)

It's a mechanical system conformed by two gears interconnected by a toothed belt and fixed to a platform. The belt moves a carriage along a vertical bar serving as a guide. Additionally, we included a sample holder attached to a horizontal bar on the carriage to secure the substrates. A stepper motor, connected to one of the gear wheels, enables the movement of the system.

The sample holders were designed in the form of a clothespin consisting of three parts (Fig. 3a). Two of these parts act as the arms that hold the substrates, which have an identical shape and connect by a fulcrum. We designed the arms in two variations: one to hold a single sample (Fig. 3c) and the other to hold two samples simultaneously, allowing them to be placed side by side (Fig. 3d). The third part of the sample holder keeps the arms together and applies the necessary pressure to maintain the system connected and secure the samples in place.

We also designed two variants of the pressure piece to accommodate one (Fig. 3e) or two samples (Fig. 3f), positioning them facing each other. In this way, through a lever action, when pressing the two tips at the top of the arms, the tips open, and when released, the third piece applies the pressure that closes the two tips, creating the necessary action to effectively hold the samples.

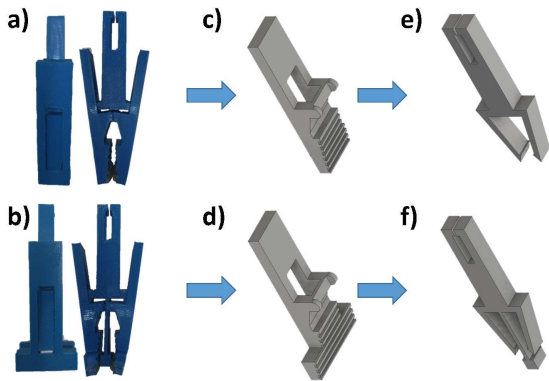


Figure 3. Representation and images of the sample holder. Photos of the two functional clip versions (a,b). Arms of the clip (c,d). Piece that provides closing pressure (e,f).

For manufacturing the pieces, we utilized an FDM (Fused Deposition Modeling) 3D printer, specifically the Ender-3 model from CREALITY-3D. The software used to generate the layers was supplied by the same company. The parts were created using Polylactic Acid (PLA) in the form of 1.75 mm diameter filaments, commercially provided by 3DBots [11]. This technology significantly reduced the cost of the prototype and showcased its advantages for future project production.

This subsystem enabled us to have precise control over the immersion and extraction speed of the substrates from the solutions. Additionally, the design significantly reduced the movement-related issues associated with the sample holder.

II.2. Subsystem for selecting the precursor solution to be used (Figure 2b)

Drawing from the concept of a carousel, since it was straightforward to implement, we opted to arrange the required solution containers on a circular acrylic platform fixed to a metal base, as depicted in Fig. 2b. At the center of this platform, a gear is securely attached. Furthermore, a stepper motor is fixed to the base and connected to the acrylic platform gear via a toothed transmission chain.

The principle of operation of this device is based on the movement of the stepper motor. When activated, the stepper motor rotates its gear, which is transmitted through the toothed transmission chain to the central gear of the acrylic plate. This rotational movement allows the platform to rotate around its center.

In this way, the device provides precise and adjustable control for the rotation of the platform. By varying the direction and speed of the stepper motor, the rotation of the platform can be

controlled at different angles and speeds, providing versatility in its operation.

It is worth mentioning that initially, the system was constructed with a gear transmission system. These gears were made from the same acrylic material as the base and cut using laser technology. During system testing, we observed that small defects in the gear radius caused two effects on the system's rotation. One was significant vibration throughout the platform and consequently on the solutions placed on it. The other effect was the system stopping due to the intense pressure exerted between the gears. We decided to separate the gears and eliminate or mitigate their defects by switching to a chain transmission system. This modification resulted in a smooth movement without vibrations that could impact the growth system's performance.

We printed the chain (Fig. 4a)) using the same plastic material and the same 3D printer that was used to fabricate the sample holders. To achieve this goal, we modified a design found on the website [12] and fabricated each link one by one. A complete link was made by three principal parts (Fig. 4b): the side plates, pins, and rollers. The side plates are the outer parts of the links and are connected through the cylindrical pins. They are designed to protect the internal components of the chain and also provide stability and strength to the chain. The rollers are mounted on the pins and roll on the teeth of the gear. The Fig. 4c is a photo of a printed and functional link and the chain is formed connecting each link one by one.

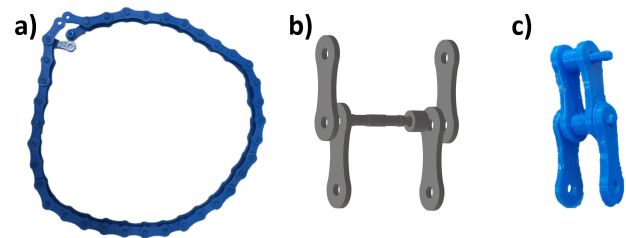


Figure 4. Representation and images of a link in the chain. a) Photo of the printed chain. b) Design of a link to form the entire chain. c) Photo of a printed link.

The platform was divided into eight sections where we could place the containers, one per section. The containers are securely fastened with radial metal rods to prevent any lateral movement. We securely fixed one end of the rods to the center of the base, while the opposite end was inserted into a PLA piece that glides smoothly along the edge of the circumference (see Fig. 2b top view). This design allowed us to accommodate containers of various sizes and shapes, and therefore different volumes.

II.3. Control subsystem for communication between the computer and the device (Figure 2c)

We utilized an Arduino UNO R3 programmable microcontroller as the basis for the control and power subsystem of the two stepper motors. This microcontroller has 14 digital input/output pins that provide a 5 V voltage

regardless of the type of power supply connected to Arduino. We were able to control the movement of the motors according to the requirements of the SILAR automated system by connecting the motor coil wires to the output pins and implementing a suitable program.

To bridge the voltage gap between the 5 V output pins of the Arduino and the 12 V requirement of the stepper motors, we integrated an Adafruit Motor Shield into the circuit setup. This shield, connected to the Arduino, facilitated the direct powering of the stepper motors at the necessary voltage level. By utilizing the functionalities of the Motor Shield, we achieved precise and independent control over two stepper motors, ensuring efficient operation. Subsequently, we focused on developing a user-friendly interface by utilizing Arduino's serial communication ports to enable seamless bidirectional interaction with a computer interface. By implementing the PyQt framework, a Python adaptation of the Qt graphical library, users could easily enter growth parameters on the computer and transfer them to Arduino for automated processes. The pySerial library was instrumental in managing the serial port communication on the computer, enhancing port control for the system's operation and feedback display. The resulting graphical user interface (GUI) provided a streamlined experience for users, emphasizing ease of use and efficient parameter modification for optimal system performance.

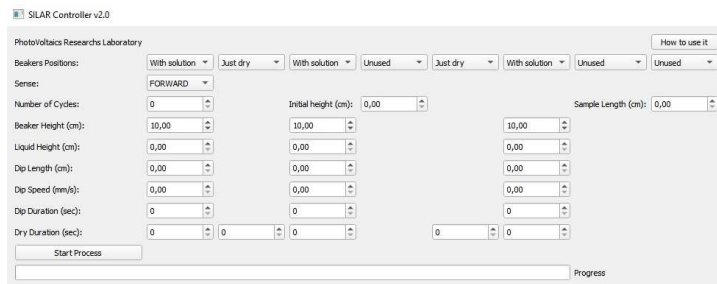


Figure 5. User interface screenshot.

The user interface allowed us to easily modify the growth parameters and send the initial system configuration to Arduino. Moreover, we successfully established a seamless data exchange between the board and the computer. This accomplishment was crucial, enabling us to accurately track the system's current cycle, which was previously challenging. With this new functionality, we now have clear and real-time visibility of the system's state at all times.

We have made the plans for each part of the system publicly accessible on our website (https://github.com/ernestomas/SILAR_V1). This includes the Arduino and Python codes that enable serial communication and facilitate the development of the user interface. By openly sharing these resources, we invite collaboration and encourage others to build upon our work.

III. SYSTEM VALIDATION

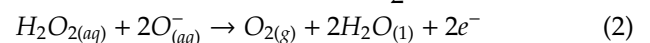
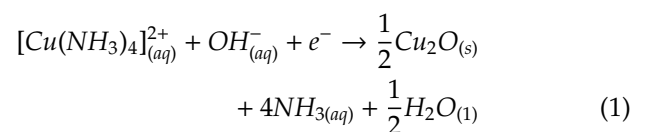
To validate the automation of the technique and optimize the growth process parameters of the equipment, we proposed conducting the deposition of copper oxides thin films. We opted for this approach based on the successful utilization of SILAR-grown layers in photovoltaic devices, as demonstrated in a previous study [13].

The first step was to identify an appropriate chemical route to grow the desired layers. In the study conducted by Chatterjee et al [13] they successfully deposited Cu_2O using the SILAR technique at room temperature and pressure. Then they annealed the Cu_2O samples to obtain the CuO films. Given the results of their method, we decided to replicate it for our project and compare the film's properties to validate our system.

To obtain the Cu_2O thin film using SILAR a combination of precursor solutions was used. Copper (II) chloride dihydrate ($CuCl_2 \cdot 2H_2O$) was used as salt precursor of copper(II), ammonium hydroxide (NH_3) acted as the complexing agent, and hydrogen peroxide (H_2O_2) served as the oxidizing agent. Methanol at 98 % (CH_3OH) was utilized as the solvent.

For the preparation of the cationic precursor, copper (II) chloride dihydrate was dissolved in methanol. Subsequently, NH_3 (25 %) was added to adjust the pH to approximately 10. We achieved a final solution volume of 250 ml and a concentration of 0.1 M. The solution of methanol and copper(II) chloride exhibited a light green color. However, the introduction of NH_3 led to a noticeable color change in the solution, turning it into a deep blue shade. This transformation indicates the formation of the $[Cu(NH_3)_4]^{2+}$ complex.

The formation of Cu_2O by reduction and the consequent oxidation of hydrogen peroxide are represented in the following half-equations:



The reducing solution was prepared by combining 2 ml of H_2O_2 (1 %) with methanol, resulting in a total volume of 200 ml. This mixture successfully yielded the desired reducing solution. Methanol was used for the subsequent washing process after each immersion in the reducing solution and cationic precursor.

Using the automated equipment, we carried out the deposition process at room temperature and pressure. Each SILAR cycle involves four steps. During the first step, the substrates (we use microscope glass slices) were vertically immersed in the cationic precursor solution for 30 seconds, allowing the adsorption of copper ions. Subsequently, a 20-second immersion in methanol was performed to remove unadsorbed ions. This step played a crucial role in achieving acceptable sample homogeneity.

In the third step, the substrates were immersed in the H_2O_2 solution for 10 seconds to reduce the copper ions adsorbed during the first step. Finally, the washing process from the second step was repeated before initiating a new cycle. The SILAR cycle was repeated 12 times for each sample. With each cycle, it became increasingly evident that the sample was progressively darkening, indicating the material deposition. Subsequently, each sample was annealed at $170\text{ }^\circ\text{C}$ in an ambient environment to evaporate residual solvents.

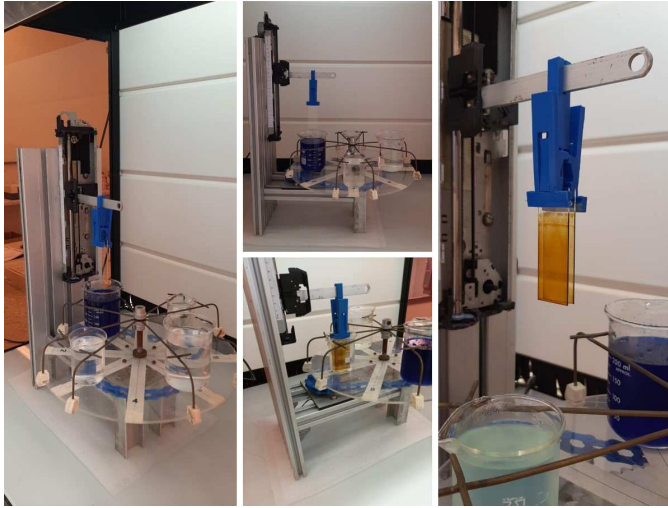


Figure 6. Collage of images of the system during a deposition procedure.

To convert copper(I) oxide (Cu_2O) into copper(II) oxide (CuO), the sample was annealed at $450\text{ }^\circ\text{C}$. This method of conversion has been previously documented [14, 15], which shows that at temperatures above $400\text{ }^\circ\text{C}$, the CuO phase begins to dominate due to the oxidation of Cu_2O . The process was conducted at ambient pressure, and upon completion, the sample exhibited a darker color compared to the non-oxidized samples, indicating a change in the material's bandgap value.

To confirm the presence of the desired phase oxides, we performed an analysis using X-ray diffraction (XRD) collected on a powder X-ray diffractometer (Empyrean, Anton Paar) in $\theta - 2\theta$ configuration, with $Cu\text{ K}\alpha$ radiation ($\lambda = 1.54052\text{ \AA}$) at 40 kV, and 30 mA, and a 0.013 step size of 2θ angle from 10 to 100. The obtained results for the as grown sample and CuO sample are shown in Fig. 7 from bottom to the top, respectively. In the as grown samples diffractogram, no intensity peaks were observed. On the other hand, intensity peaks corresponding to the CuO phases are observed in the CuO sample (Fig. 7) matching the CuO diffraction pattern extracted from JCPDS #41-0254.

The absence of peaks in the as grown sample may be related to the small size of the coherence domains formed using the SILAR technique, making its crystal structure undetectable by X-ray diffraction. However, it may also be attributed to the amorphous nature of the sample as it grows. Upon subjecting the samples to heat treatment, larger crystals form, enabling the crystal structure to be resolved through X-ray diffraction. Similar behavior has been previously observed by Rafea et al. [16], who studied the influence of post-growth annealing

on Cu_2O samples obtained by the SILAR technique.

We used the Scherrer equation $D_{hkl} = \frac{K\lambda}{\beta \cos \theta}$ to measure the crystallite size in the direction perpendicular to the lattice planes with Miller index (hkl) from CuO X-ray diffractograms. The sizes calculated over the three more intense peaks were 29, 25 y 21 nm, respectively.

We analyze images of the samples using a Scanning Electron Microscope (SEM). These images are shown in Fig. 8, revealing a significant change in the morphology of the samples (Fig. 8a.1 and 8b.1), but not in the films thickness (Fig. 8a.2 and 8b.2).

The as grown sample displayed a compact layer composed by very small nanoparticles compared to those forming the CuO sample. The presence of fine grains in the sample provides further support for the hypothesis derived from the XRD findings, indicating that the small size of the coherence domains is responsible for the lack of distinct peaks in the diffractogram of the as-grown sample.

The average size of the CuO nanoparticles, measured in SEM images, has been determined to be 23 nm, which is in good agreement with the size calculated using the Scherrer equation.

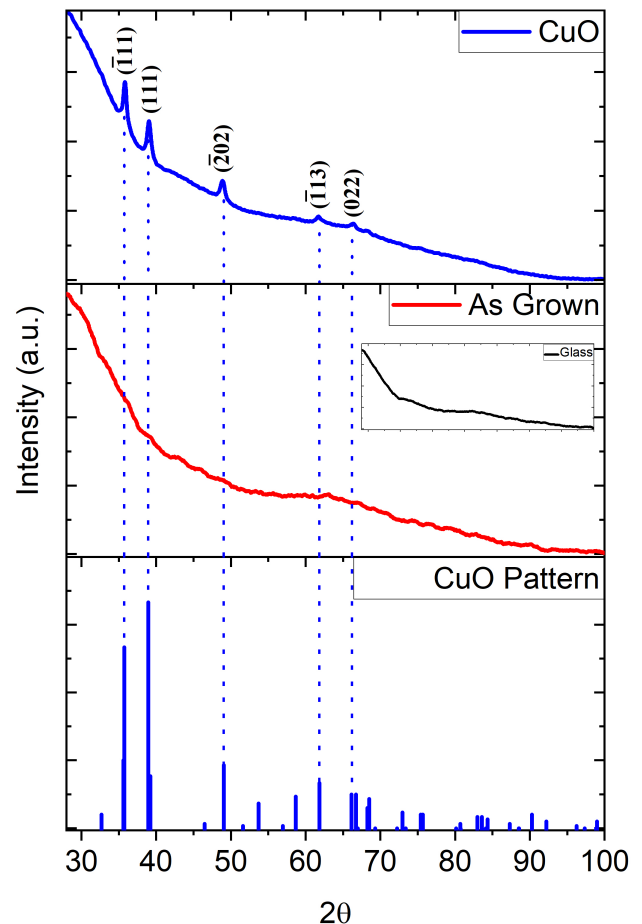


Figure 7. X ray diffractograms of the substrate, as grown, and CuO samples.

were determined to be 1.48 and 2.24 eV, respectively (values closely aligned with those reported in the literature [19]).

IV. CONCLUSIONS

We report the successful development of a low-cost automated system that effectively synthesizes high-quality micro and nanostructures using the SILAR method. Through design optimization and implementation of innovative solutions such as the use of 3D printing and the reuse of old printer systems, the system operates efficiently. The use of both recycled parts and those fabricated by additive manufacturing using local facilities has proven to be a highly effective strategy in reducing costs and maximizing overall system efficiency. The integration of Arduino and Motor Shield was crucial in achieving simultaneous motor control and complete automation of the deposition process. Moreover, the project benefited from the availability of free software for controlling the integrated circuits and user interface design tools. This access to cost-effective solutions greatly facilitated the development of the system, making it both practical and economical. Using this equipment, nanostructured films of semiconductor oxides were successfully obtained to evaluate their potential use in photovoltaic devices. The deposited layers successfully validated the automated version of the developed SILAR method.

V. ACKNOWLEDGMENTS

The authors would like to thank funding from the projects: Low-cost nanostructured solar cells: a prototype for Cuba (Cuba-Nanosolar) belonging to the National Nanoscience and Nanotechnologies Program in Cuba and the FOURIER Project "Strengthening universities and research centers in renewable energy sources", from the European Program of Aid to the Energy in Cuba.

REFERENCIAS

- [1] D. Mitzi, "Solution processing of inorganic materials", (John Wiley & Sons, 2008).
- [2] K. L. Chopra, and I. Kaur, "Thin Film Device Applications", 1st edition, (Springer, 1983).
- [3] D. Perednis, and L. J. Gauckler, J. Electroceram. **14**, 103 (2005).
- [4] A. Jilani, M. S. Abdel-Wahab and A. H. Hammad, Modern Technol. Creating Thin-film Syst. Coat. **2**, 137 (2017).
- [5] S. P. Ratnayake, J. Ren, E. Colusso, M. Guglielmi, A. Martucci, and E. Della Gaspera, Small **17**, 2101666 (2021).
- [6] T. P. Niesen, and M. R. De Guire, J. Electroceram. **6**, 169 (2001).
- [7] J. R. Arthur, "Specimen handling, preparation, and treatments in surface characterization", (Springer, 1998)
- [8] Y. Nicolau, Appl. Surf. Sci. **22**, 1061 (1985).
- [9] J. Puetz, and M. Aegerter, "Dip Coating Technique. In: Aegerter, M.A., Mennig, M. (eds) Sol-Gel Technologies for Glass Producers and Users", (Springer, Boston, 2004).
- [10] X. Tang, and X. Yan, J. Sol-Gel Sci. Technol. **81**, 378 (2017).

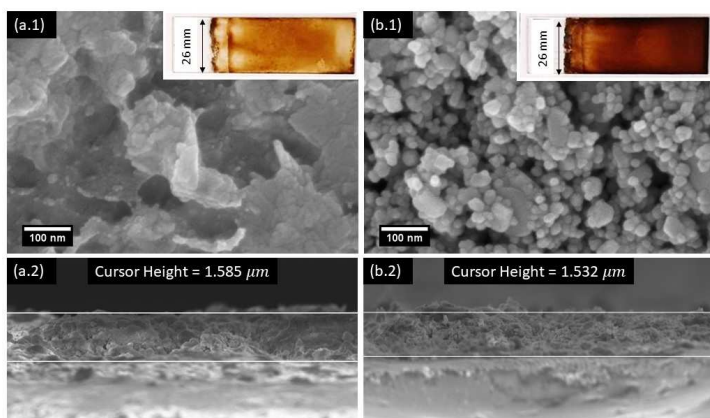


Figure 8. Top-view (a.1) and cross-sectional (a.2) SEM images of the as grown sample. Top-view (b.1) and cross-sectional (b.2) SEM images of the CuO sample. Each top-view SEM image includes an inset photo of the sample.

To further validate the formation of semiconductor oxides using an optical technique, UV-Vis spectroscopy was employed. The spectrometer Cary 5000 with an acquisition range of 200-3300 nm was used in absorbance mode at room temperature. Fig. 9 displays the plots of the absorption coefficient curves as a function of photon energy. By employing the Tauc method [17], the band gap values for CuO and Cu₂O were determined.

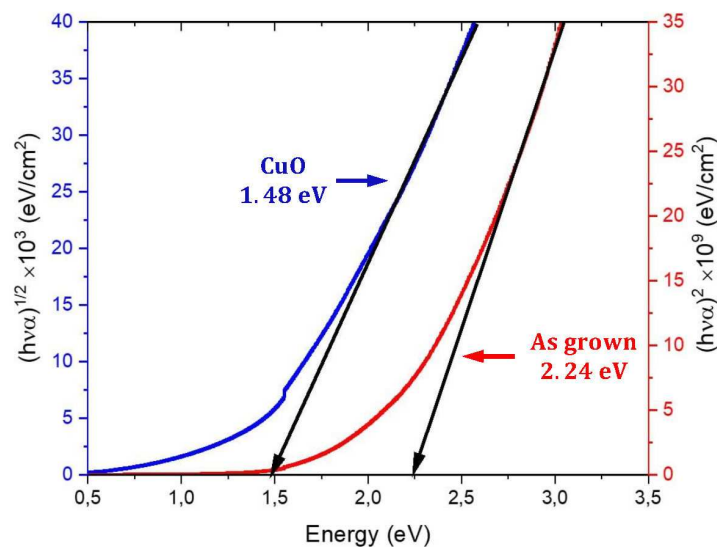


Figure 9. Tauc plots of as grown and CuO thin films.

The Cu₂O and CuO has a direct band gap, but some studies have reported an indirect band gap for CuO [18]. To further investigate this behavior, we adjusted the Tauc plot for the CuO sample to account for both types of transitions. Fig. 9 displays the plots of $h\nu\alpha$, with an exponent of 1/2 (blue axis) and with an exponent of 2 (red axis) correspondent to an indirect and a direct transition respectively. We have presented the fit for the smallest bandgap CuO value, which turned out to be the indirect one. The band gap values for CuO and Cu₂O

- [11] URL https://3dbots.co/producto/filamento_pla/, visited on 15/9/2023.
- [12] Kylekorn, Bike chain mechanism/chain drive. URL <https://www.thingiverse.com/thing:223602>, visited on 12/8/2023.
- [13] S. Chatterjee, S. K. Saha, and A. J. Pal, Sol. Energy Mat. Sol. Cells **147**, 17 (2016).
- [14] N. Serin, T. Serin, S. Horzum, and Y. Celik, Semicond. Sci. Technol. **20**, 398 (2005).
- [15] S. C. Ray, Sol. Energy Mat. Sol. Cells **68**, 307 (2001).
- [16] M. A. Rafe,a and N. Roushdy, J. Phys. D: Appl. Phys. **42**, 015413 (2008).
- [17] P. Samanta, A. Saha, and T. Kamilya, J. Nano- and Electron. Phys. **6**, 04015-1 (2014).
- [18] A. Rydosz, K. Kollbek, N.-T. H. Kim-Ngan, A. Czapla, and A. Brudnik, J. Mat. Sci.: Mat. Electron. **31**, 11624 (2020).
- [19] C. G. Ribbing, and A. Roos, E. D. Palik, "Handbook of Optical Constants of Solids", (Academic Press, Burlington, 1997).

This work is licensed under the Creative Commons Attribution-NonCommercial 4.0 International (CC BY-NC 4.0, <http://creativecommons.org/licenses/by-nc/4.0>) license.

